Published in final edited form as:
Sci Signal. ; 2(87): ra51. doi:10.1126/scisignal.2000396.

Proteomic Analysis of Integrin-Associated Complexes Identifies RCC2 as a Dual Regulator of Rac1 and Arf6

Jonathan D. Humphries[1,2,*], **Adam Byron**[1,2,*], **Mark D. Bass**[1,2], **Sue E. Craig**[1,2], **John W. Pinney**[2,†], **David Knight**[2], and **Martin J. Humphries**[1,2,‡]

[1]Wellcome Trust Centre for Cell-Matrix Research, University of Manchester, Manchester M13 9PT, UK

[2]Faculty of Life Sciences, University of Manchester, Manchester M13 9PT, UK

Abstract

The binding of integrin adhesion receptors to their extracellular matrix ligands controls cell morphology, movement, survival, and differentiation in various developmental, homeostatic, and disease processes. Here, we report a methodology to isolate complexes associated with integrin adhesion receptors, which, like other receptor-associated signaling complexes, have been refractory to proteomic analysis. Quantitative, comparative analyses of the proteomes of two receptor-ligand pairs, $\alpha_4\beta_1$–VCAM-1 and $\alpha_5\beta_1$–fibronectin, defined both core and receptor-specific components. Regulator of chromosome condensation-2 (RCC2) was detected in the $\alpha_5\beta_1$–fibronectin signaling network at an intersection between the Rac1 and Arf6 sub-networks. RCC2 knockdown enhanced fibronectin-induced activation of both Rac1 and Arf6 and accelerated cell spreading, suggesting that RCC2 limits the signaling required for membrane protrusion and delivery. Dysregulation of Rac1 and Arf6 function by RCC2 knockdown also abolished persistent migration along fibronectin fibers, indicating a functional role for RCC2 in directional cell movement. This proteomics workflow now opens the way to further dissection and systems-level analyses of adhesion signaling.

INTRODUCTION

Multicellular existence relies on the engagement of integrin cell surface receptors with the extracellular matrix (ECM) and counter-receptors on adjacent cells. Integrins are a family of 24 αβ heterodimers that result from selective non-covalent associations of 18 α and 8 β subunits (1, 2). All subunits comprise large extracellular and typically small cytoplasmic domains. The particular combination of extracellular domains determines ligand-binding specificity, the structural basis of which enables the family to be subdivided into four main classes (3). RGD-binding integrins, including all five α_V integrins, two β_1 integrins (α_5 and α_8), and $\alpha_{IIb}\beta_3$, share the ability to recognise ligands such as fibronectin (FN), vitronectin, and fibrinogen, which contain the RGD tripeptide motif. LDV-binding integrins $\alpha_4\beta_1$, $\alpha_4\beta_7$, $\alpha_9\beta_1$, and the four members of the β_2 subfamily recognise active sites containing LDV-related sequences in ligands such as vascular cell adhesion molecule-1 (VCAM-1), mucosal addressin cell adhesion molecule-1 (MAdCAM-1), and intercellular cell adhesion molecule-1 (ICAM-1). A-domain-containing β_1 integrins (α_1, α_2, α_{10}, and α_{11}) bind laminin and collagen, whereas the non-αA-domain-containing laminin-binding integrins,

‡To whom correspondence should be addressed. martin.humphries@manchester.ac.uk.
*These authors contributed equally to this work.
†Present address: Centre for Bioinformatics, Division of Molecular Biosciences, Imperial College London, London SW7 2AZ, UK.

Supplementary Material: www.sciencesignaling.org/cgi/content/full/2/87/ra51/DC1

Europe PMC Funders Author Manuscripts

comprising three β_1 integrins (α_3, α_6, and α_7) and $\alpha_6\beta_4$, are highly selective laminin receptors.

Integrin-ligand binding controls a diverse range of cellular functions in both health and disease and is orchestrated by a combination of membrane-associated signaling complexes and mechanosensitive connections to the actin cytoskeleton (4-6). Approximately 150 components of integrin signaling complexes have been described, and based on their reported pairwise interactions, a hypothetical integrin 'adhesome' has been created (7). However, the networks that translate ligand binding into functional readouts, the extent of receptor-specific and spatiotemporal variation in composition, the stoichiometry of complex components, and the molecular mechanisms that coordinate different pathways within the signaling network are unknown. To date, systematic global analyses of the integrin signaling nexus have been hampered by the inherent lability and inaccessibility of plasma membrane-associated complexes. Here, we report the development of a quantitative proteomic methodology suitable for the analysis of transmembrane receptor-ligand complexes, and the application of the methodology to two related, but functionally distinct, integrin-ligand pairs: $\alpha_4\beta_1$–VCAM-1 and $\alpha_5\beta_1$–FN. These structurally related integrins were selected because they have been reported to exhibit distinct functional activities with respect to cell migration and exertion of cellular contractile forces (8, 9). We reasoned that their proteomes would contain both shared and receptor-specific interacting proteins.

RESULTS

A quantitative proteomic methodology for the analysis of integrin adhesion complexes

Integrin-associated complexes were isolated from α_5^+/α_4^+ K562 cells (K562 cells stably transfected with α_4 integrin) using a ligand affinity purification approach (Fig. 1A). α_5^+/α_4^+ K562 cells display a similar degree of attachment to VCAM-1 compared to that mediated by endogenous $\alpha_5\beta_1$ to FN and demonstrate similar activation-state modulation of $\alpha_4\beta_1$ compared to that of the endogenously expressed receptor (10). The restricted integrin expression profile of α_5^+/α_4^+ K562 cells, unlike most other cells, thus enabled heterodimer-specific adhesion and signaling events to be pinpointed.

Paramagnetic beads were coated with integrin ligands (FN for $\alpha_5\beta_1$ or VCAM-1 for $\alpha_4\beta_1$) and mixed with cells in suspension to induce the formation of adhesion complexes. Following sonication and detergent extraction, bead-associated material was probed for the presence of integrin subunits and the adhesion complex components talin and paxillin by Western blotting. Consistent with previous attempts to identify integrin-associated proteins by immunoprecipitation, low amounts of talin and paxillin were recovered (Fig. 1, B and C). However, the addition of the membrane-permeable cross-linker dimethyl-3,3′-dithiobispropionimidate (DTBP) prior to cell lysis increased the recovery of adhesion complex components compared to the controls, which were anti–transferrin receptor (TfR) antibody or a VCAM-1 $Asp^{40}\rightarrow$Ala (D40A) mutant that does not bind to integrins. In contrast, the non-membrane-permeable cross-linker 3,3′-dithiobis(sulfosuccinimidylpropionate) (DTSSP) increased the recovery of the primary receptor-ligand complex, but failed to retain talin and paxillin (Fig. 1B). Disruption of the actin cytoskeleton with cytochalasin D did not affect the recovery of talin and paxillin, demonstrating that the integrin-associated complexes were not simply trapped in an extended actin network (fig. S1). Taken together, these data demonstrate that specific and efficient isolation of integrin-associated complexes is possible, but that it requires use of a membrane-permeable cross-linker prior to cell lysis.

Tandem mass spectrometry identified with ≥99% confidence 620, 418, and 319 proteins in FN, VCAM-1, and non-integrin-binding control samples, respectively. Of the characterized

FN receptors (3), α_5 was the predominant α integrin subunit detected in FN-induced complexes, whereas β_3 integrin was not detected. In addition, $\alpha_4\beta_1$ was the only integrin receptor detected in VCAM-1-induced complexes. These data demonstrate that the complexes isolated by FN and VCAM-1 are primarily recruited by $\alpha_5\beta_1$ and $\alpha_4\beta_1$ integrins, respectively.

Relative abundance of identified proteins was measured using spectral counting (11, 12). Hierarchical clustering was used to identify patterns of recruitment of proteins between samples and to aid the objective assimilation of multiple, large proteomic datasets (13) (Fig. 2 and table S1). Unbiased Pearson correlation identified five major groups of proteins based on their relative abundance in the different samples, which corresponded to clusters of proteins enriched to VCAM-1 (correlation = 0.66), FN (correlation = 0.72), both FN and VCAM-1 (correlation = 0.71), the negative control (correlation = 0.64), or all three conditions (correlation = 0.65) (displayed from top to bottom, respectively, in Fig. 2A). We reasoned that the groups identified by hierarchical clustering represented proteins that were either specifically enriched in $\alpha_5\beta_1$–FN or $\alpha_4\beta_1$–VCAM-1 complexes, were core components of both types of complex, or were non-specifically recruited. As an important test of the unbiased clustering, the α_4 and α_5 integrin subunits were found to reside, as expected, in clusters enriched in VCAM-1 and FN samples, respectively (Fig. 2, B and C). Known adhesion complex proteins, including myosin IIA, vinculin, VASP (vasodilator-stimulated phosphoprotein), filamin, ACF7 (actin cross-linking family protein 7), IQGAP (IQ motif–containing GTPase-activating protein), Rap1b, and protein phosphatase 2, were found in a dual FN- and VCAM-1-enriched cluster, characterized by a higher abundance of the proteins in the FN samples compared to VCAM-1 samples (Fig. 2D). The shared β_1 integrin subunit resided in a separate dual FN- and VCAM-1-enriched cluster (Fig. 2E), along with several well-characterized adhesion complex proteins, including kindlin-3, talin-1, zyxin, fascin, α-actinin-4, moesin, 14-3-3 protein β/α, myosin IIB, and actin-related protein (Arp) 2/3 complex subunit 3 (Fig. 2E and tables S1 and S2). The proteins identified in the dual FN- and VCAM-1-enriched clusters can therefore be considered core components of the two complexes.

Analysis of the clusters specifically enriched to either integrin ligand revealed a much larger number of proteins enriched in FN samples compared to VCAM-1, suggesting that FN has a greater agonistic potential to recruit the adhesion machinery than VCAM-1 (Fig. 2, B and C, and tables S1 and S2). For FN, this cluster again contained several well-studied adhesion complex proteins including CD98hc (cluster of differentiation 98 heavy chain), ILK (integrin-linked kinase), LASP1 [LIM (Lin-11, Isl-1, and Mec-3) and SH3 (Src homology 3) protein 1], disabled-2, Arp2/3 complex components, and 14-3-3 proteins, but it also contained many candidate adhesion components. The smaller VCAM-1 cluster contained proteins such as ADP-ribosylation factor (Arf) 1, SHP2 [SH2 (Src homology 2) domain–containing protein tyrosine phosphatase 2], and casein kinase 1 that were detected exclusively in VCAM-1 samples, as well as a group of proteins (including galectin-1, Rab5C, and Rac1) that were detected in both integrin ligands but enriched in VCAM-1 compared to FN samples. Intriguingly, some proteins that have been documented as components of mature integrin-containing adhesion complexes, such as tensin, FAK (focal adhesion kinase), p130Cas, and Src, were not identified in our analyses. A distinguishing feature of these proteins is that they are responsive to the application of force (2, 4, 14-16), and their absence is consistent with the fact that bead-bound complexes were isolated without the specific application of tension. A similar pattern of recruitment was observed for small signaling GTPases. Rac1, which drives adhesion intiation, was detected but RhoA, which is activated by force and drives the maturation of adhesion complexes (17), was not. Taken together, these findings suggest that the complex components listed in Fig. 2 and tables S1 and S2 represent early nascent adhesions. In the future, it will be important to

adapt the workflow to isolate complexes from adherent cells or from cells in suspension to which force has been applied.

FN- and VCAM-1-induced integrin interaction networks

To interrogate the molecular organization of the isolated adhesion complexes, we used protein interaction network analysis. To convert the lists of integrin-associated complex components into interaction networks, a subtractive proteomic strategy was employed. Only proteins enriched at least two-fold over the amount in non-integrin-binding control samples (406 for FN and 185 for VCAM-1; table S2) were mapped onto an interactome constructed from a union of human protein interaction datasets (18-20) and the literature-curated interactome of integrin adhesion complexes (7). The integrin-associated interaction networks were unlikely to be generated by chance as they were distinctly non-random, with significantly higher numbers of interactions and clustering coefficients than those observed for control simulations (table S3). For proteins that directly interact with β_1 integrin (the 1-hop neighborhood), an increased number mapped onto the $\alpha_5\beta_1$–FN network compared to the $\alpha_4\beta_1$–VCAM-1 network (16 compared to 9 proteins), consistent with the conclusions drawn from Fig. 2. As a result, the 2-hop neighborhood of $\alpha_5\beta_1$ was far more expansive than that of $\alpha_4\beta_1$ (34 compared to 12 proteins; Fig. 3). The fact that fewer $\alpha_4\beta_1$–VCAM-1-specific proteins were identified is consistent with previous studies that suggest $\alpha_4\beta_1$ forms weaker cytoskeletal interactions, resulting in diminished adhesion complex formation, and is therefore specialized for highly motile cell types (8, 21).

Additional normalization of quantitative MS data (to the β_1 integrin spectral count) and coloring proteins (nodes) by fold enrichment to $\alpha_5\beta_1$–FN (red) or $\alpha_4\beta_1$–VCAM-1 (blue) allowed changes in relative abundance of protein recruitment between $\alpha_5\beta_1$ and $\alpha_4\beta_1$ to be assessed. The $\alpha_5\beta_1$ network is predominantly composed of proteins specifically enriched to FN over VCAM-1, whereas the $\alpha_4\beta_1$ network consists of proteins more evenly balanced in this respect (Fig. 3). In addition, core β_1 integrin interactions identified by hierarchical clustering (Fig. 2) are common to both ligand-occupied $\alpha_5\beta_1$ and $\alpha_4\beta_1$, although the relative abundance of the core interactors within these adhesion complexes can differ. Furthermore, some well-characterized adhesion complex components, including talin, kindlin-3, α-actinin, and zyxin, are recruited to the same extent to $\alpha_4\beta_1$–VCAM-1 and $\alpha_5\beta_1$–FN (white, pale blue, or pale red nodes in Figs. 3 and 4). Thus, the reduced number of proteins detected in $\alpha_4\beta_1$–VCAM-1 complexes is due to the lack of recruitment of specific proteins, rather than an overall reduction in the amount of the components or affinity differences between the integrins and their ligands. The differences in ‘flavors’ of integrin complexes observed here reveal surprisingly diverse heterodimer-specific β_1 integrin signaling events and provide a powerful tool for the future analysis of context-specific integrin adhesion signaling.

Role of regulator of chromosome condensation-2 (RCC2) in FN-dependent adhesion complex formation, cell spreading, and migration

Examination of the integrin-ligand interaction networks revealed proteins situated at nodal points that connected identifiable signaling sub-networks. Among these proteins, RCC2, a molecule that has not previously been linked to integrin signaling, occupied a key position between the β_1 integrin, Rac1, and Arf6 1-hop neighborhoods of the $\alpha_5\beta_1$–FN network (Fig. 4A). Rac1 was detected in both $\alpha_5\beta_1$–FN and $\alpha_4\beta_1$–VCAM-1 samples but enriched in $\alpha_4\beta_1$–VCAM-1 (blue node with black border; Fig. 4A), whereas Arf6 was only detected in $\alpha_5\beta_1$–FN samples (red node with no border; Fig. 4A). RCC2 was detected in $\alpha_5\beta_1$–FN, but not $\alpha_4\beta_1$–VCAM-1 samples, by mass spectrometry, a finding confirmed by Western blotting (Fig. 4B). FN-dependent Rac1 regulation controls membrane protrusion (22, 23), and Arf6 has been implicated in integrin-dependent membrane trafficking (24). Although

little is known about RCC2, it has been reported to bind directly to the nucleotide-free form of Rac1 and speculated to act as a Rac1 guanine nucleotide exchange factor (GEF) (25). In addition, a large-scale affinity-based study mapping protein-protein interactions identified the association of RCC2 with Arf6 (26).

To test the contribution of RCC2 to FN-dependent Rac1 regulation (23, 27), RCC2 was targeted by RNA interference (RNAi). A reduction in RCC2 abundance to less than 20% had no effect on the basal Rac1 activity of cells in suspension (Fig. 4C), but surprisingly, it augmented FN-dependent activation of Rac1 (Fig. 4D). Arf6 activation assays were also performed, with RCC2 knockdown having no effect on the basal activity of Arf6 (Fig. 4E). When suspended cells adhered onto a FN substrate, a wave of Arf6 activation was induced (Fig. 4F), consistent with a previous study (24) and similar to that observed for Rac1 (Fig. 4D). Moreover, RCC2 knockdown accelerated the FN-induced wave of Arf6 activation during cell spreading (Fig. 4F). These data suggest that, rather than acting as a GEF, RCC2 limits activation of both Rac1 and Arf6.

We hypothesized that altered Rac1 and Arf6 signaling would impact cell behavior, in particular the ability to form adhesion complexes, spread, and migrate. Therefore, the effect of RCC2 on adhesion complex formation during spreading on FN was assessed (Fig. 5, A and B, and fig. S2). The total area of adhesion complexes of wild-type mouse embryonic fibroblasts (MEFs), and cells in which RCC2 had been silenced, was measured over time. Adhesion complex formation was accelerated following knockdown of RCC2, with adhesion area being significantly higher than control cells at 30 to 90 min ($P < 0.05$; Fig. 5, A and B). The period of augmented adhesion complex area coincided with the duration of enhanced Rac1 and Arf6 activities, which would be expected to augment both adhesion complex nucleation and trafficking of β_1 integrin to the membrane.

To assess the functional outcome of altered GTPase signaling upon RCC2 depletion, the spreading of MEF cells on FN, and B16-F10 mouse melanoma cells on FN or VCAM-1, was examined. Consistent with the enhanced kinetics of Rac1 and Arf6 activation, depletion of RCC2 enhanced the rate of spreading of both cell types on FN (Fig. 5, C and D, and fig. S3). B16-F10 cell spreading on VCAM-1, however, was unaffected by RCC2 knockdown (Fig. 5D and fig. S3), consistent with the recruitment of RCC2 to $\alpha_5\beta_1$–FN but not to $\alpha_4\beta_1$–VCAM-1 complexes.

A key functional readout of altered GTPase signaling upon knockdown of RCC2 was obtained by examining the migration of MEF cells on pre-formed, fibrous cell-derived matrices. Cells plated on such matrices normally migrate with a high degree of directional persistence (23, 28). In comparison to control cells, RNAi directed against RCC2 reduced persistent migration by 50% (Fig. 5, E and F). RCC2 knockdown did not, however, affect total distance moved (Fig. 5G). Taken together, these data demonstrate that RCC2 is a functionally relevant component of the machinery required to maintain persistent migration in response to an extracellular matrix cue, and intriguingly that this role is mediated by limiting the activity of Rac1 and Arf6.

DISCUSSION

Using an integrin-targeted proteomic strategy, we have identified RCC2 as a component of FN-induced signaling pathways that regulate directional cell migration. RCC2 has been previously characterized as a passenger protein, localizing to the centromere during specific stages of the cell cycle. RCC2 is required for alignment of chromosomes on the spindle (chromosome congression), centromeric targeting of the chromosome passenger complex (CPC), and activation of Aurora-B kinase, the catalytic subunit of the CPC (25, 29). The

CPC functions to regulate chromosomal and cytoskeletal events during cell division, and CPC proteins have well-defined roles in cell cleavage (30). It is therefore likely that RCC2 is also essential for cell cleavage. RCC2 shares structural homology with other RCC1 family GEFs that act on Ran, Arf1, and Rab proteins, but it is unique among this family with respect to its ability to bind Rac1 (25, 31). Inactivation of Rac is essential for cytokinesis (32) and it is becoming increasingly apparent that integrins help determine the orientation of cytokinesis and subsequent positioning of daughter cells (33, 34). How integrin signaling and the activity of RCC2 are spatiotemporally regulated during cell adhesion, spreading, and mitosis remains to be resolved, and it is intriguing that RCC2 colocalizes at the midbody with talin, an integrin-binding cytoskeletal protein, during cytokinesis (35).

Intriguingly, as well as identifying a large number of known adhesion-related components, our analyses have highlighted numerous putative novel integrin-associated proteins. For example, many proteins with functions relating to protein translation were found to be specifically enriched to FN, VCAM-1, or both integrin ligands. In support of this finding, the translational machinery has been shown to reposition to sites of adhesion (36), and β_1 integrin was found to be required to stimulate FN-mediated translation in fibroblasts (37). Moreover, we detected LIM domain–containing proteins, such as the integrin-associated proteins zyxin and paxillin, which can bind nucleic acids and thus may serve a scaffolding role in translational processes (36). Furthermore, a quantitative proteomics approach identified ribonucleoprotein complexes, likely to be involved in protein translation, which appeared during early stages of cell spreading at locations close to sites of adhesion (38).

In summary, this first non-candidate-based analysis of integrin ligand-induced signaling has identified core and receptor-specific components of $\alpha_5\beta_1$ and $\alpha_4\beta_1$ integrin signaling complexes and pinpointed RCC2 as a coordinator of FN-dependent adhesion signaling pathways, a dual activity-limiter of Rac1 and Arf6, and a regulator of adhesion complex formation, cell spreading, and directional migration. The abundance of active Rac1 governs the persistence of cell migration through the formation of peripheral lamellae (28). We speculate that RCC2 acts to restrict activation of Rac1 and Arf6 to a degree that enables effective membrane protrusion and integrin trafficking, thereby permitting cells to both maintain directional migration and respond to the topographic features of their environment. The development of this proteomics pipeline now allows the molecular composition of various adhesion complexes to be measured directly, and opens the way to systems-level analyses of adhesion.

MATERIALS AND METHODS

Reagents

Human plasma FN was purchased from Sigma-Aldrich (Poole, UK). Fc-tagged recombinant soluble VCAM-1, comprising immunoglobulin (Ig) domains 1 and 2, and mutant VCAM-1(D40A), containing a D40A point mutation in the integrin-binding site and termed control throughout this study, were expressed from the pIG1 vector and purified as described (39).

Monoclonal antibodies used were mouse anti–human β_1 integrin (JB1A; provided by J. A. Wilkins, University of Manitoba, Winnipeg, MB, Canada), mouse anti–human paxillin (clone 349; BD Biosciences, Oxford, UK), mouse anti–human vinculin (hVIN-1; Sigma-Aldrich), mouse anti–human TfR (H68.4; Invitrogen, Paisley, UK), mouse anti–human TfR (OKT9; European Collection of Cell Cultures, Porton Down, UK), mouse anti-Rac1 (BD Biosciences), mouse anti-Arf6 (Sigma-Aldrich), and mouse anti–human mitochondrial heat shock protein 70 kD (Hsp70) (JG1; ABR–Affinity BioReagents, Golden, CO, USA). Polyclonal antibodies used were goat anti–human α_4 integrin (C-20; Santa Cruz

Biotechnology, Santa Cruz, CA, USA), rabbit anti–human α_5 integrin (H-104; Santa Cruz Biotechnology), goat anti–human β_1 integrin (N-20; Santa Cruz Biotechnology), goat anti–human talin (C-20; Santa Cruz Biotechnology), and rabbit anti-RCC2 (Bethyl Laboratories, Montgomery, TX, USA). Other antibodies used were donkey anti–goat IgG or donkey anti–mouse IgG conjugated to Alexa Fluor 680 (Invitrogen) and donkey anti–mouse IgG or donkey anti–rabbit IgG conjugated to IRDye 800 (Rockland Immunochemicals, Gilbertsville, PA, USA).

Cell culture

K562 human chronic myelogenous leukemia cells stably transfected with α_4 integrin (α_5^+/α_4^+ K562 cells) were a gift from M. E. Hemler (Dana-Farber Cancer Institute, Boston, MA, USA) and were cultured in RPMI 1640 medium supplemented with 10% (v/v) fetal calf serum (FCS; Lonza Bioscience, Wokingham, UK), 2 mM L-glutamine, and 1 mg/ml Geneticin (Invitrogen). The generation of immortalized MEF cells has been described previously (23). To allow expression of the large T antigen, MEF cells were cultured at 33°C in Dulbecco's modified Eagle's medium (DMEM; Sigma-Aldrich) supplemented with 10% (v/v) FCS, 2 mM L-glutamine, and 20 U/ml interferon-γ (Sigma-Aldrich). B16-F10 mouse melanoma cells were cultured in DMEM supplemented with 10% (v/v) FCS and 2 mM L-glutamine. All cell lines were maintained at 37°C in a humidified 5% (v/v) CO_2 atmosphere, unless otherwise stated.

Ligand affinity purification assay

The isolation of plasma membrane fractions enriched for integrin membrane complexes was based upon the protocol of Plopper and Ingber (40), modified here to permit the isolation of integrin-associated protein complexes for proteomic analysis. Ligand or antibody was coupled to tosyl-activated paramagnetic Dynabeads M-450 (4.5 μm diameter; Invitrogen) as described in the manufacturer's protocol. For FN-coated beads, beads were incubated with 0.125 mM bis(sulfosuccinimidyl) suberate cross-linker (Thermo Fisher Scientific, Waltham, MA, USA) for 15 min at 25°C to increase covalent bond formation between FN and beads. Coated beads were incubated with α_5^+/α_4^+ K562 cells in DMEM containing 25 mM *N*-2-hydroxyethylpiperazine-*N*′-2-ethanesulfonic acid (HEPES), 4.5 mg/ml glucose, and L-glutamine (DMEM/HEPES) (Invitrogen) supplemented with 0.2% (w/v) BSA and 0.4 mM $MnCl_2$ at 70 r.p.m. for 30 min at 37°C. DTBP or DTSSP cross-linker (Thermo Fisher Scientific) in DMEM/HEPES was added to bead-bound cells to a final concentration of 3 mM, where applicable, and samples were incubated for a further 30 min at 37°C (70 r.p.m.). Cross-linker was quenched with 20 mM Tris-HCl before isolation of bead-bound cells on a magnet. Samples were washed with CSK buffer [10 mM piperazine-*N*,*N*′-bis(2-ethanesulfonic acid), pH 6.8, 50 mM NaCl, 150 mM sucrose, 3 mM $MgCl_2$, 1 mM $MnCl_2$] supplemented with 20 mM Tris-HCl, pH 8.5, and 2 mM Na_3VO_4. Cells were lysed in CSK^+ buffer [CSK buffer supplemented with 0.5% (w/v) Triton X-100, 10 μg/ml leupeptin, 10 μg/ml aprotinin, 0.5 mM 4-(2-aminoethyl)benzenesulfonyl-fluoride hydrochloride (AEBSF), 2 mM Na_3VO_4] for 30 min on ice with sonication (VibraCell VCX 500, Sonics & Materials, Newtown, CT, USA). Following cell lysis, beads were washed with CSK^+ buffer, and affinity-purified proteins were eluted from beads with reducing sample buffer [50 mM Tris-HCl, pH 6.8, 10% (w/v) glycerol, 4% (w/v) sodium dodecylsulfate (SDS), 0.004% (w/v) bromophenol blue, 8% (v/v) β-mercaptoethanol]. Protein samples were separated from beads using a magnet, resolved by SDS–polyacrylamide gel electrophoresis (PAGE), and analyzed by Coomassie staining or Western blotting (see supplementary methods).

Mass spectrometry and data analysis

Details of the mass spectrometry and data analysis are provided in the supplementary methods.

RNAi of RCC2

siRNA duplexes targeting mouse RCC2, sequence (sense) CCAACGUGGUGGUUCGAGA (with ON TARGET modification for enhanced specificity), and non-targeting control duplex were purchased from Dharmacon (Thermo Fisher Scientific). Oligo (0.8 nmol) was transfected into a 90% confluent 75-cm^2 flask of MEF or B16-F10 mouse melanoma cells using Lipofectamine 2000 reagent (Invitrogen). After 24 hours, the cells were passaged and retransfected to achieve a reduction in expression to below 20%. Cells were passaged and then cultured for a further 24 hours before use. For each experiment, RCC2 abundance was tested by Western blotting.

GTPase activity, adhesion area measurement, cell spreading, and cell migration assays

Details of the Rac1 and Arf6 activity assays, adhesion area quantification, and cell spreading and migration assays are provided in the supplementary methods.

Supplementary Material

Refer to Web version on PubMed Central for supplementary material.

Acknowledgments

We thank S. Warwood (University of Manchester) for MS data acquisition, A. G. Garrow (Unilever, Sharnbrook, UK) for providing the human protein interaction data sets, J. N. Selley (University of Manchester) for bioinformatic support, E.-J. Keevil (University of Manchester) for assistance with MS sample preparation, J. Kott (University of Manchester) for assistance with microscopy, J. A. Askari (University of Manchester) for discussions, and A. D. Sharrocks, C. Ballestrem, C. H. Streuli, R. A. North, and N. Papalopulu (all University of Manchester) for critical reading of the manuscript. This work was supported by grants 045225 and 074941 from the Wellcome Trust (to M.J.H.) and by a Biotechnology and Biological Sciences Research Council (BBSRC) Collaborative Awards in Science and Engineering PhD studentship, sponsored by GlaxoSmithKline (A.B.). The Biomolecular Analysis Facility mass spectrometer and Bioimaging Facility microscopes used in this study were purchased with grants from the BBSRC, Wellcome Trust, and the University of Manchester Strategic Fund.

REFERENCES AND NOTES

1. Hynes RO. Integrins: Bidirectional, allosteric signaling machines. Cell. 2002; 110:673–687. [PubMed: 12297042]
2. Arnaout MA, Goodman SL, Xiong J-P. Structure and mechanics of integrin-based cell adhesion. Curr. Opin. Cell Biol. 2007; 19:495–507. [PubMed: 17928215]
3. Humphries JD, Byron A, Humphries MJ. Integrin ligands at a glance. J. Cell Sci. 2006; 119:3901–3903. [PubMed: 16988024]
4. Geiger B, Bershadsky A, Pankov R, Yamada KM. Transmembrane crosstalk between the extracellular matrix and the cytoskeleton. Nat. Rev. Mol. Cell Biol. 2001; 2:793–805. [PubMed: 11715046]
5. Delon I, Brown NH. Integrins and the actin cytoskeleton. Curr. Opin. Cell Biol. 2007; 19:43–50. [PubMed: 17184985]
6. Legate KR, Fässler R. Mechanisms that regulate adaptor binding to β-integrin cytoplasmic tails. J. Cell Sci. 2009; 122:187–198. [PubMed: 19118211]
7. Zaidel-Bar R, Itzkovitz S, Ma'ayan A, Iyengar R, Geiger B. Functional atlas of the integrin adhesome. Nat. Cell Biol. 2007; 9:858–867. [PubMed: 17671451]
8. Chan BMC, Kassner PD, Schiro JA, Byers HR, Kupper TS, Hemler ME. Distinct cellular functions mediated by different VLA integrin α subunit cytoplasmic domains. Cell. 1992; 68:1051–1060. [PubMed: 1547502]
9. Liu S, Thomas SM, Woodside DG, Rose DM, Kiosses WB, Pfaff M, Ginsberg MH. Binding of paxillin to α4 integrins modifies integrin-dependent biological responses. Nature. 1999; 402:676–681. [PubMed: 10604475]

10. Humphries JD, Schofield NR, Mostafavi-Pour Z, Green LJ, Garratt AN, Mould AP, Humphries MJ. Dual functionality of the anti-β_1 integrin antibody, 12G10, exemplifies agonistic signalling from the ligand binding pocket of integrin adhesion receptors. J. Biol. Chem. 2005; 280:10234–10243. [PubMed: 15632175]
11. Liu H, Sadygov RG, Yates JR III. A model for random sampling and estimation of relative protein abundance in shotgun proteomics. Anal. Chem. 2004; 76:4193–4201. [PubMed: 15253663]
12. Dong M-Q, Venable JD, Au N, Xu T, Park SK, Cociorva D, Johnson JR, Dillin A, Yates JR III. Quantitative mass spectrometry identifies insulin signaling targets in C. elegans. Science. 2007; 317:660–663. [PubMed: 17673661]
13. Eisen MB, Spellman PT, Brown PO, Botstein D. Cluster analysis and display of genome-wide expression patterns. Proc. Natl. Acad. Sci. U.S.A. 1998; 95:14863–14868. [PubMed: 9843981]
14. Wang H-B, Dembo M, Hanks SK, Wang Y-L. Focal adhesion kinase is involved in mechanosensing during fibroblast migration. Proc. Natl. Acad. Sci. U.S.A. 2001; 98:11295–11300. [PubMed: 11572981]
15. Friedland JC, Lee MH, Boettiger D. Mechanically activated integrin switch controls α5β1 function. Science. 2009; 323:642–644. [PubMed: 19179533]
16. Sawada Y, Tamada M, Dublin-Thaler BJ, Cherniavskaya O, Sakai R, Tanaka S, Sheetz MP. Force sensing by mechanical extension of the Src family kinase substrate p130Cas. Cell. 2006; 127:1015–1026. [PubMed: 17129785]
17. Zhao X-H, Laschinger C, Arora P, Szaszi K, Kapus A, McCulloch CA. Force activates smooth muscle α-actin promoter activity through the Rho signaling pathway. J. Cell Sci. 2007; 120:1801–1809. [PubMed: 17456553]
18. Rual J-F, Venkatesan K, Hao T, Hirozane-Kishikawa T, Dricot A, Li N, Berriz GF, Gibbons FD, Dreze M, Ayivi-Guedehoussou N, Klitgord N, Simon C, Boxem M, Milstein S, Rosenberg J, Goldberg DS, Zhang LV, Wong SL, Franklin G, Li S, Albala JS, Lim J, Fraughton C, Llamosas E, Cevik S, Bex C, Lamesch P, Sikorski RS, Vandenhaute J, Zoghbi HY, Smolyar A, Bosak S, Sequerra R, Doucette-Stamm L, Cusick ME, Hill DE, Roth FP, Vidal M. Towards a proteome-scale map of the human protein–protein interaction network. Nature. 2005; 437:1173–1178. [PubMed: 16189514]
19. Stelzl U, Worm U, Lalowski M, Haenig C, Brembeck FH, Goehler H, Stroedicke M, Zenkner M, Schoenherr A, Koeppen S, Timm J, Mintzlaff S, Abraham C, Bock N, Kietzmann S, Goedde A, Toksöz E, Droege A, Krobitsch S, Korn B, Birchmeier W, Lehrach H, Wanker EE. A human protein–protein interaction network: A resource for annotating the proteome. Cell. 2005; 122:957–968. [PubMed: 16169070]
20. Ramani AK, Bunescu RC, Mooney RJ, Marcotte EM. Consolidating the set of known human protein-protein interactions in preparation for large-scale mapping of the human interactome. Genome Biol. 2005; 6:R40. [PubMed: 15892868]
21. Kassner PD, Alon R, Springer TA, Hemler ME. Specialized functional properties of the integrin α4 cytoplasmic domain. Mol. Biol. Cell. 1995; 6:661–674. [PubMed: 7579686]
22. Price LS, Leng J, Schwartz MA, Bokoch GM. Activation of Rac and Cdc42 by integrins mediates cell spreading. Mol. Biol. Cell. 1998; 9:1863–1871. [PubMed: 9658176]
23. Bass MD, Roach KA, Morgan MR, Mostafavi-Pour Z, Schoen T, Muramatsu T, Mayer U, Ballestrem C, Spatz JP, Humphries MJ. Syndecan-4-dependent Rac1 regulation determines directional migration in response to the extracellular matrix. J. Cell Biol. 2007; 177:527–538. [PubMed: 17485492]
24. Balasubramanian N, Scott DW, Castle JD, Casanova JE, Schwartz MA. Arf6 and microtubules in adhesion dependent trafficking of lipid rafts. Nat. Cell Biol. 2007; 9:1381–1391. [PubMed: 18026091]
25. Mollinari C, Reynaud C, Martineau-Thuillier S, Monier S, Kieffer S, Garin J, Andreassen PR, Boulet A, Goud B, Kleman J-P, Margolis RL. The mammalian passenger protein TD-60 is an RCC1 family member with an essential role in prometaphase to metaphase progression. Dev. Cell. 2003; 5:295–307. [PubMed: 12919680]
26. Ewing RM, Chu P, Elisma F, Li H, Taylor P, Climie S, McBroom-Cerajewski L, Robinson MD, O'Connor L, Li M, Taylor R, Dharsee M, Ho Y, Heilbut A, Moore L, Zhang S, Ornatsky O,

Bukhman YV, Ethier M, Sheng Y, Vasilescu J, Abu-Farha M, Lambert JP, Duewel HS, Stewart II, Kuehl B, Hogue K, Colwill K, Gladwish K, Muskat B, Kinach R, Adams SL, Moran MF, Morin GB, Topaloglou T, Figeys D. Large-scale mapping of human protein-protein interactions by mass spectrometry. Mol. Syst. Biol. 2007; 3:89. [PubMed: 17353931]

27. del Pozo MA, Alderson NB, Kiosses WB, Chiang H-H, Anderson RGW, Schwartz MA. Integrins regulate Rac targeting by internalization of membrane domains. Science. 2004; 303:839–842. [PubMed: 14764880]
28. Pankov R, Endo Y, Even-Ram S, Araki M, Clark K, Cukierman E, Matsumoto K, Yamada KM. A Rac switch regulates random versus directionally persistent cell migration. J. Cell Biol. 2005; 170:793–802. [PubMed: 16129786]
29. Rosasco-Nitcher SE, Lan W, Khorasanizadeh S, Stukenberg PT. Centromeric Aurora-B activation requires TD-60, microtubules, and substrate priming phosphorylation. Science. 2008; 319:469–472. [PubMed: 18218899]
30. Carmena M. Cytokinesis: The final stop for the chromosomal passengers. Biochem. Soc. Trans. 2008; 36:367–370. [PubMed: 18481960]
31. Rosa JL, Casaroli-Marano RP, Buckler AJ, Vilaro S, Barbacid M. p619, a giant protein related to the chromosome condensation regulator RCC1, stimulates guanine nucleotide exchange on ARF1 and Rab proteins. EMBO J. 1996; 15:4262–4273. [PubMed: 8861955]
32. Canman JC, Lewellyn L, Laband K, Smerdon SJ, Desai A, Bowerman B, Oegema K. Inhibition of Rac by the GAP activity of centralspindlin is essential for cytokinesis. Science. 2008; 322:1543–1546. [PubMed: 19056985]
33. Streuli CH. Integrins and cell-fate determination. J. Cell Sci. 2009; 122:171–177. [PubMed: 19118209]
34. Reverte CG, Benware A, Jones CW, LaFlamme SE. Perturbing integrin function inhibits microtubule growth from centrosomes, spindle assembly, and cytokinesis. J. Cell Biol. 2006; 174:491–497. [PubMed: 16908668]
35. Bellissent-Waydelich A, Vanier M-T, Albigès-Rizo C, Simon-Assmann P. Talin concentrates to the midbody region during mammalian cell cytokinesis. J. Histochem. Cytochem. 1999; 47:1357–1368. [PubMed: 10544209]
36. Chicurel ME, Singer RH, Meyer CJ, Ingber DE. Integrin binding and mechanical tension induce movement of mRNA and ribosomes to focal adhesions. Nature. 1998; 392:730–733. [PubMed: 9565036]
37. Gorrini C, Loreni F, Gandin V, Sala LA, Sonenberg N, Marchisio PC, Biffo S. Fibronectin controls cap-dependent translation through β_1 integrin and eukaryotic initiation factors 4 and 2 coordinated pathways. Proc. Natl. Acad. Sci. U.S.A. 2005; 102:9200–9205. [PubMed: 15961545]
38. de Hoog CL, Foster LJ, Mann M. RNA and RNA binding proteins participate in early stages of cell spreading through spreading initiation centers. Cell. 2004; 117:649–662. [PubMed: 15163412]
39. Newham P, Craig SE, Seddon GN, Schofield NR, Rees A, Edwards RM, Jones EY, Humphries MJ. α4 integrin binding interfaces on VCAM-1 and MAdCAM-1. Integrin binding footprints identify accessory binding sites that play a role in integrin specificity. J. Biol. Chem. 1997; 272:19429–19440. [PubMed: 9235944]
40. Plopper G, Ingber DE. Rapid induction and isolation of focal adhesion complexes. Biochem. Biophys. Res. Commun. 1993; 193:571–578. [PubMed: 7685596]

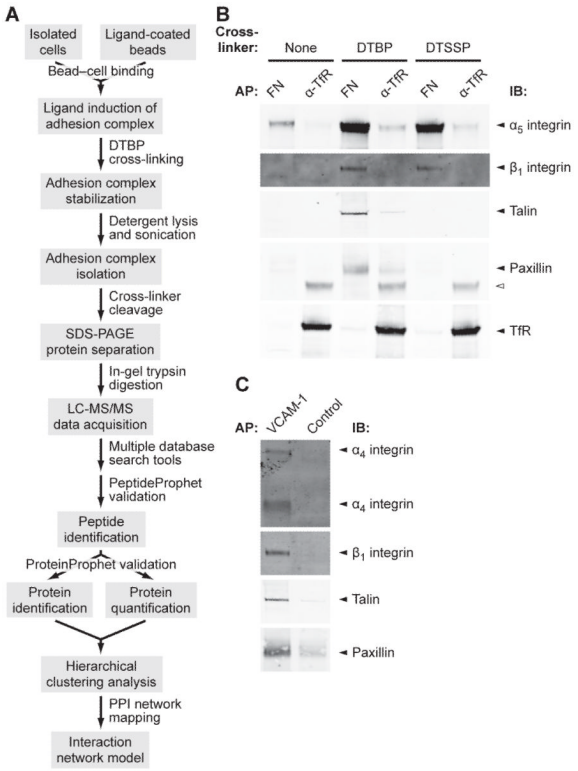

Fig. 1.

A quantitative proteomic pipeline for the analysis of integrin adhesion complexes. (**A**) Schematic workflow of the ligand affinity isolation strategy in conjunction with MS data acquisition, validation, and interpretation. (**B** and **C**) The specific nature of the isolated integrin ligand complexes was demonstrated by Western blotting, as compared with control pulldowns (α-TfR, transferrin receptor antibody; Control, non-integrin-binding VCAM-1 D40A mutant). $\alpha_5\beta_1$–FN cytoskeletal complexes were isolated using the cell membrane–permeable cross-linker DTBP but not the cell membrane–impermeable cross-linker DTSSP (B), and $\alpha_4\beta_1$–VCAM-1 cytoskeletal complexes were isolated with DTBP (C). Bead-coated proteins used for each affinity purification (AP) and proteins probed for by immunoblotting (IB) are indicated. Mouse IgG fragments are indicated by a white arrowhead.

Europe PMC Funders Author Manuscripts

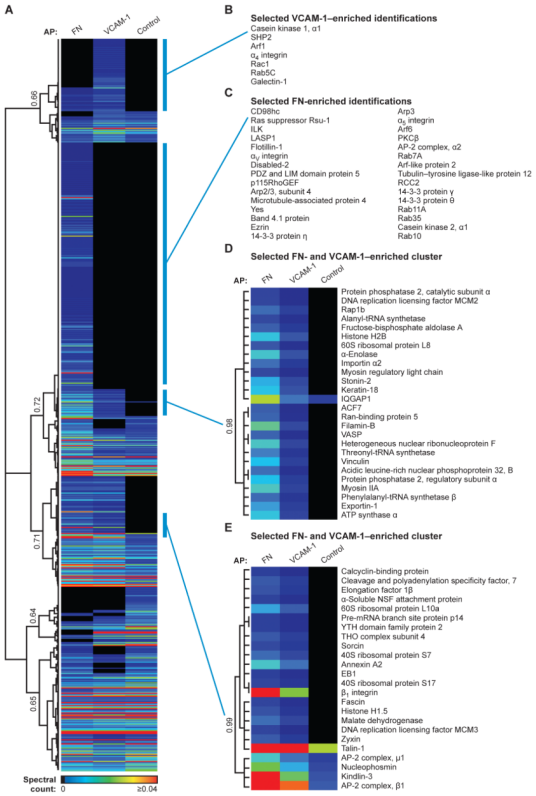

Fig. 2.

Hierarchical clustering of proteins identified by MS analysis of FN, VCAM-1, and control affinity purifications. (**A**) Complete output of unsupervised hierarchical clustering analysis of identified proteins. Quantitative heat maps display mean spectral counts as a percentage of the total number of spectra identified in each analysis. Associated dendrograms display hierarchical clustering on the basis of uncentered Pearson correlation using complete linkage. Correlations at selected nodes are indicated. (**B** to **E**) Selected ligand-specific and core β_1 integrin–enriched proteins are displayed, indicated by blue bars in (A).

Europe PMC Funders Author Manuscripts

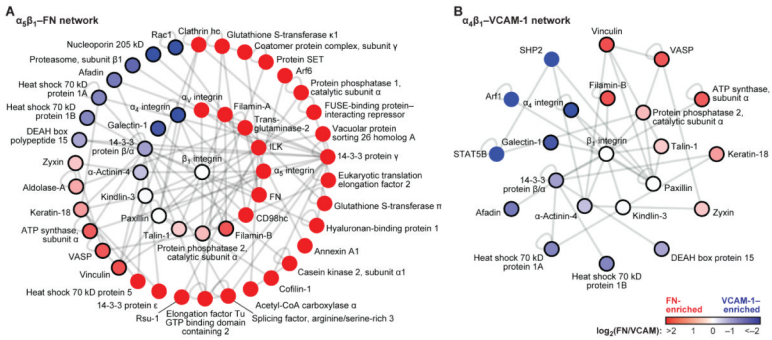

Fig. 3.

Protein–protein interaction network models for $\alpha_5\beta_1$–FN and $\alpha_4\beta_1$–VCAM-1 complexes. (**A** and **B**) Proteins identified in $\alpha_5\beta_1$–FN (A) and $\alpha_4\beta_1$–VCAM-1 (B) complexes after a subtractive proteomics strategy were mapped onto a human interactome to generate interaction network models. Proteins identified within two path lengths (the 2-hop neighborhood) of β_1 integrin are shown, with the 1- and 2-hop neighborhoods forming the inner and outer circles, respectively. Protein identifications (nodes) are colored according to their relative enrichment to $\alpha_5\beta_1$–FN (red) or $\alpha_4\beta_1$–VCAM-1 (blue) and are ordered in a clockwise fashion relating to their relative enrichment to $\alpha_5\beta_1$–FN. Proteins identified in both $\alpha_5\beta_1$–FN and $\alpha_4\beta_1$–VCAM-1 datasets are indicated by a black node border; absence of a black border indicates unique identification in that integrin-ligand dataset.

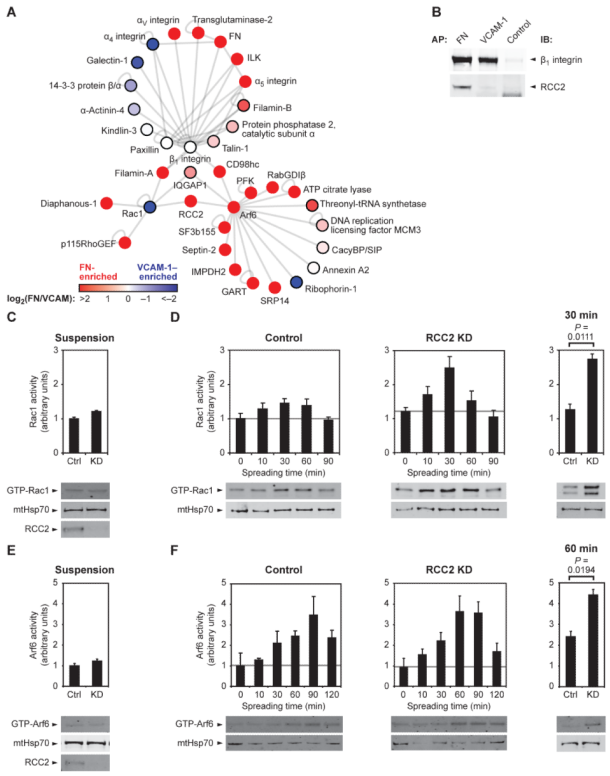

Fig. 4.

Recruitment of RCC2 to FN-bound complexes modulates the activation of Rac1 and Arf6. (**A**) A focused view of the $\alpha_5\beta_1$–FN network, highlighting the intersection of the β_1 integrin, Rac1, and Arf6 1-hop neighborhoods. Protein identifications are colored as described in Fig. 3. Abbreviations: CacyBP/SIP, calcyclin-binding protein/Siah-1–interacting protein; GART, trifunctional purine biosynthetic protein adenosine-3; GDI, GDP dissociation inhibitor; IMPDH2, inosine monophosphate dehydrogenase 2; PFK, phosphofructokinase-1; SF3b155, splicing factor 3b, subunit 1, 155 kD; SRP14, signal recognition particle 14 kD. (**B**) Verification of the specific recruitment of RCC2 to $\alpha_5\beta_1$–FN complexes by Western blotting. (**C** to **F**) The activities of Rac1 (C and D) and Arf6 (E and F) were measured by effector pulldown assays in combination with quantitative Western blotting using fluorophore-conjugated antibodies. Activities were compared between control and RCC2-knockdown cells in suspension (C and E) or during spreading on FN (D and F). Equivalent loading between experiments was confirmed by blotting crude lysates for mitochondrial Hsp70. Axes are in arbitrary units assigned according to the relative activity of cells in suspension. Each panel is representative of at least four separate experiments. Error bars indicate standard error of the mean (SEM); *P* values were calculated for direct comparisons of peak time points using a Student's *t*-test, as indicated.

Europe PMC Funders Author Manuscripts

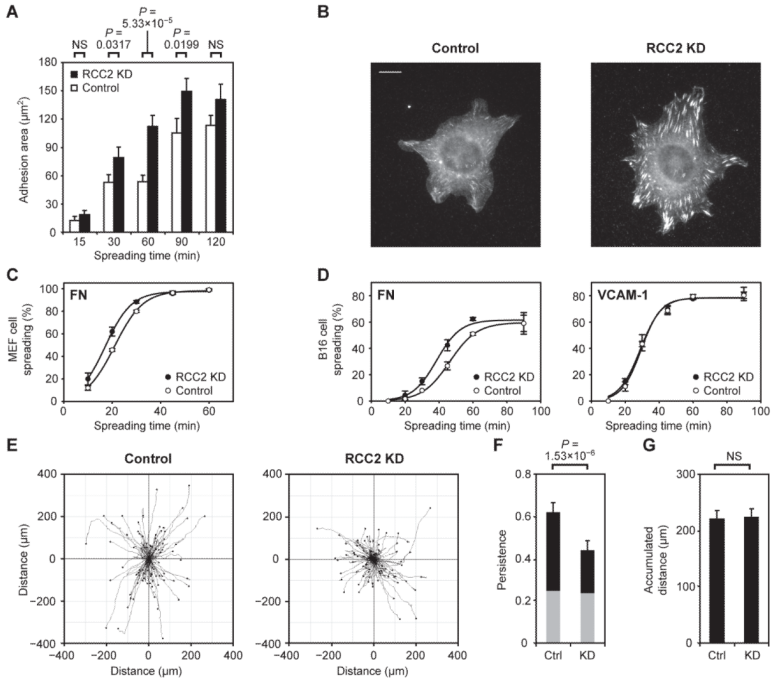

Fig. 5.

RCC2 modulates FN-dependent adhesion complex formation, cell spreading, and directional migration. (**A** and **B**) Adhesion complex formation during spreading of control and RCC2-knockdown MEF cells on FN. Cells were fixed at the indicated times and stained for vinculin to permit measurement of focal adhesion area using ImageJ software (A). Forty-five cells were analyzed for each cell type at each time point. Data are representative of two independent experiments. Images shown are representative of cells that were allowed to spread for 60 min (B). (**C** and **D**) Spreading of cells transfected with control or RCC2 siRNAs. The percentage of MEF cells on FN (C) or B16-F10 cells on FN or VCAM-1 (D) counted as spread was plotted as a function of time. The shifts in the measure of half-maximal cell spreading (control minus RCC2-knockdown; mean ± standard deviation) were as follows: MEF cells spread on FN, 3.21 ± 0.68 min (14.9 ± 2.5% acceleration compared to control); B16 cells spread on FN, 8.34 ± 2.44 min (14.1 ± 2.9% acceleration compared to control); B16 cells spread on VCAM-1, −0.40 ± 1.54 min (−0.5 ± 3.3% acceleration compared to control). (**E** to **G**) Control and RCC2-knockdown MEF cell migration on cell-derived matrix. Cells were allowed to spread on cell-derived matrix for 3 hours before imaging at 10-min intervals for 12 hours. Migration paths of 90 cells for each cell type were tracked using ImageJ software (E). The tracks of cells from three different fields of view from triplicate wells have been combined into each panel. Data are representative of three independent experiments. Persistence of migration (F) was determined by dividing the linear displacement of a cell by the total distance moved (accumulated distance; G). Grey blocks represent the experimentally determined threshold for the random migration of cells on FN. Error bars indicate SEM; *P* values were determined using a *Z*-test, as indicated.

Europe PMC Funders Author Manuscripts